

# Sensitivity analysis on chaotic dynamical system by Non-Intrusive Least Square Shadowing (NILSS)

Angxiu Ni<sup>a,\*</sup>, Qiqi Wang<sup>a</sup>

<sup>a</sup>*Aeronautics and Astronautics, MIT, 77 Mass Ave, Cambridge, MA 02139, USA*

---

## Abstract

This paper develops the tangent Non-Intrusive Least Square Shadowing (NILSS) method, which computes sensitivity for chaotic dynamical systems. In NILSS, a tangent solution is represented as a linear combination of a inhomogeneous tangent solution and some homogeneous tangent solutions. Then we solve a least square problem under this new representation. As a result, this new variant is easier to implement with existing solvers. For chaotic systems with large degrees of freedom but low dimensional attractors, NILSS has low computation cost. NILSS is applied to two chaotic PDE systems: the Lorenz 63 system, and a CFD simulation of a backward-facing step. The results show that NILSS computes the correct derivative with a lower cost than the conventional Least Square Shadowing method and the conventional finite difference method.

*Keywords:* Sensitivity analysis, linear response, tangent equation, chaos, dynamical systems, uniform hyperbolicity, ergodicity, least square shadowing

---

## 1. Introduction

Many important phenomena in engineering are chaotic, such as problems involving turbulent flows[1] or fluid-structure interactions[2]. For these chaotic systems, we are often interested in long-time averaged quantities rather than instantaneous quantities. Furthermore, we want to perform sensitivity analysis, i.e. to know how the change in the parameters of the systems would affect those long-time averaged quantities. Such sensitivity analysis is the purpose of this paper.

Consider a deterministic dynamical system parameterized by  $s$ :

$$\frac{du}{dt} = f(u, s) \quad (1)$$

Here  $f(u, s) : \mathbb{R}^m \times \mathbb{R} \rightarrow \mathbb{R}^m$  is a smooth function,  $u$  is the state. A solution  $u(t)$  is called the primal solution. The initial condition of the primal solution is  $u(t=0) = u_0$ .

---

\*Corresponding author.

*Email addresses:* niangxiu@mit.edu (Angxiu Ni), qiqi@mit.edu (Qiqi Wang)

Let  $J(u, s) : \mathbb{R}^m \times \mathbb{R} \rightarrow \mathbb{R}$  be a continuous function which defines the instantaneous objective. The averaged  $J$  over a time period of  $T$  is:

$$\langle J \rangle_T := \frac{1}{T} \int_0^T J(u, s) dt \quad (2)$$

$\langle J \rangle_T$  is a function of  $s$ ,  $u_0$ , and  $T$ . If we let  $T$  goes to infinity, then we obtain  $\langle J \rangle_\infty$ , which is only determined by  $s$  and  $u_0$ . Here we make the assumption of ergodicity [3], which means that  $u_0$  does not affect  $\langle J \rangle_\infty$ . As a result, the objective we are interested in,  $\langle J \rangle_\infty$ , is only a function of  $s$ .

We are interested in computing the sensitivity  $d\langle J \rangle_\infty / ds$ , since it is useful information in helping scientists and engineers design products [4, 5], control processes and systems [6, 7], solve inverse problems [8], estimate simulation errors [9, 10, 11], assimilate measurement data [12, 13] and quantify uncertainties [14].

However, when the dynamical system is chaotic, computing a meaningful  $d\langle J \rangle_\infty / ds$  is challenging. The conventional way includes finite difference method and the transient method, which applies conventional tangent method directly to chaotic systems. One of the new approaches is the ensemble method developed by Lea et al[15, 16]. It computes the sensitivity by averaging  $d\langle J \rangle_T / ds$  over an ensemble of trajectories. Another recent approach is based on the fluctuation dissipation theorem (FDT)[17, 18, 19, 20, 21, 22].

This paper follows the approach of Least Square Shadowing (LSS) developed by Wang, Hu and Blonigan[23, 14]. LSS first computes a bounded shift of a trajectory under parameters change, which is called LSS solution. Then we can substitute the LSS solution into the derivative of equation 2 to compute  $d\langle J \rangle_\infty / ds$ . LSS has been successfully applied to some dynamical systems such as the Lorenz 63 system and a modified Kuramoto-Sivashinsky equation[24, 14, 25]. LSS has also been applied by Blonigan et al. to engineering applications such as sensitivity analysis for airfoils[26, 25]. It has been proved by Wang that under ergodicity and hyperbolicity assumptions, LSS converges to the correct sensitivity at a rate of  $T^{-0.5}$ , where  $T$  is the trajectory time length[23].

However, for very large systems, LSS is still expensive. In the original formulation of LSS, the majority of computation comes from solving a least square problem by its KKT conditions. The number of variables is the product of the dimension of the system and the number of time steps. As the system gets larger and trajectory longer, the equation system becomes extremely large. Also, the equation system can be stiff, requiring many iterations. As a result, solving the equation system could be very expensive [26]. Furthermore, previous formulations of LSS are intrusive, requiring Jacobian matrix  $\partial_u f(u, s)$  at each time step. However, many existing simulation software may not readily provide such information, thus requiring modification to the code.

The Non-Intrusive Least Square Shadowing (NILSS) is relatively faster and easier to use than the conventional LSS method. The cost of NILSS is roughly proportional to the dimension of the attractor, which is much lower than the dimension of the system for many engineering applications. Hence NILSS could

be much cheaper to solve under this scenario. Another benefit is that the information required in NILSS can be obtained without intrusive modification to existing tangent solvers, since NILSS no longer requires  $\partial_u f(u, s)$ . NILSS does require the underlying tangent solver being able to do numerical integration starting from any initial condition, whereas most existing solvers are coded only to perform integration from zero initial condition. Nevertheless, it greatly reduces the amount of intruding, which could encourage more engineers to use this method. Also, NILSS needs to store less data than the conventional LSS. Furthermore, the formulation of NILSS allows implementation which could put most of its data onto hard drive instead of computer memory.

The rest of this paper is organized as follows: First, we address the sensitivity with respect to parameters and initial conditions, and the relation between them. Then we explain tangent NILSS method. Then we present a more detailed flowchart of tangent NI-LSS algorithm on multiple time segments. Finally, we apply tangent NILSS to the Lorenz 63 system and a CFD simulation of a flow past a backward facing step.

## 2. Sensitivity to initial conditions and parameters

Trajectories of chaotic dynamical systems depends sensitively on its parameters. Change the parameters of the governing equation by a small amount, the new trajectory will grow further apart from the old one, even though they start from the same initial condition. This is similar to the better known ‘butterfly effects’, which is the sensitive dependence on the initial condition. It means that for chaotic systems, a small difference in the initial condition can result in a large difference later on.

For example, the Lorenz 63 system is a simplified ODE model for atmospheric convection[27]. It has three state parameters  $x, y, z$  and a parameter  $\rho$ . In figure 1 we show the sensitive dependence of trajectories on both the initial condition and the parameter. For the left column, we plot on the  $x$ - $z$  plane  $1.8 \times 10^7$  trajectories with the same initial condition but different  $\rho$ . Here  $\rho$  is uniformly distributed between 27.999 and 28.001: smaller  $\rho$  is indicated by colors with shorter wavelength (blue), while larger  $\rho$  by longer wavelength (red). On the right column, we plot the same number of trajectories with the same parameter  $\rho = 28$  but slightly different initial conditions  $u_0$ .

As we can see in the first three pictures on the left, changing  $s$  has is similar to changing  $\rho$ : All these trajectories part from each other in a very similar way. Eventually, as shown in the last picture on the left, all trajectories settle into distribution similar to the attractor on the right. However, notice that the last figure on the left has different colors in different parts: the upper rim of is red, and the lower rim is blue. This is due to that the figure is the superposition of many attractors with different parameters. Red colors correspond to attractors with a large  $\rho$ . So the red shade on the upper rim indicates that as we increase  $\rho$ , the attractor moves upward in the  $z$  direction. This means that  $\langle z \rangle_\infty$  may have a positive and well-defined sensitivity with respect to  $\rho$ .

Hence changing  $\rho$  has two effects. In the short time, it results in diverging trajectories which looks exactly like only changing  $u_0$ . In the long time, it results in a shifted attractor. The latter effect is hidden under the diverging trajectories and is only visible after a long time. However, it is the shift in the attractor that we want for computing the sensitivity. Our main goal in this paper, is to devise an algorithm such that we can ‘subtract’ the effect of changing  $u_0$  from that of changing  $\rho$ , so that we can obtain the shift of the attractor. We will solidify above qualitative description in later sections.

### 3. Explanation of tangent NI-LSS

In this section we provide an explanation of tangent NI-LSS. First we describe the two effects of changing parameters, as mentioned in the last section. Then we see why  $V^\perp$ , the subspaces perpendicular to  $f$ , has its own Lyapunov Characteristic Vectors (LCV). Then we see how NI-LSS formulate the desired tangent solution from 1) a particular tangent solution  $v^*$ , and 2) several homogeneous solutions  $\{w_j\}$ . Finally, we look at how to compute  $d\langle J \rangle_\infty / ds$  from tangent solutions. Also, Appendix A explains the derivation of  $d\langle J \rangle_\infty / ds$ .

#### 3.1. Two effects of a parameter perturbation

Assume the dynamical system in equation (1) has an infinitesimal perturbation  $\Delta s$  in the parameter, the new parameter is  $s + \Delta s$ . The new solution is denoted by  $u + \Delta u$ , which satisfy:

$$\frac{d(u + \Delta u)}{dt} = f(u + \Delta u, s + \Delta s)$$

Subtract by equation (1) and neglect second order small quantities. Let  $v = \Delta u / \Delta s$ , since  $\Delta s$  is infinitesimal,  $v = du/ds$ .  $v$  satisfies the following tangent equation:

$$\frac{dv}{dt} - \partial_u f v = \partial_s f \quad (3)$$

Here  $\partial_u f$  is a  $\mathbb{R}^m \times \mathbb{R}^m$  matrix and  $\partial_s f$  is a  $\mathbb{R}^m$  column vector.

This  $v$  is undetermined unless a initial condition is specified. Conventionally, zero initial condition is used. We denote  $v^*$  as the solution of equation 3 with the initial condition  $v^*(t = 0) = 0$ .  $v^*$  is also the solution of conventional tangent method, its zero initial condition is due to that we assume  $u_0$  is unchanged. Hence  $v^*$  characterizes the kind of perturbation in the left column of figure 1.

If there is a small perturbation in  $u_0$  but no perturbation in  $s$ , the new solution satisfies:

$$\frac{du + \Delta u}{dt} = f(u + \Delta u, s)$$

Through the same deduction, denote  $w = du/ds$ , it satisfies the homogeneous tangent equation:

$$\frac{dw}{dt} - \partial_u f w = 0 \quad (4)$$

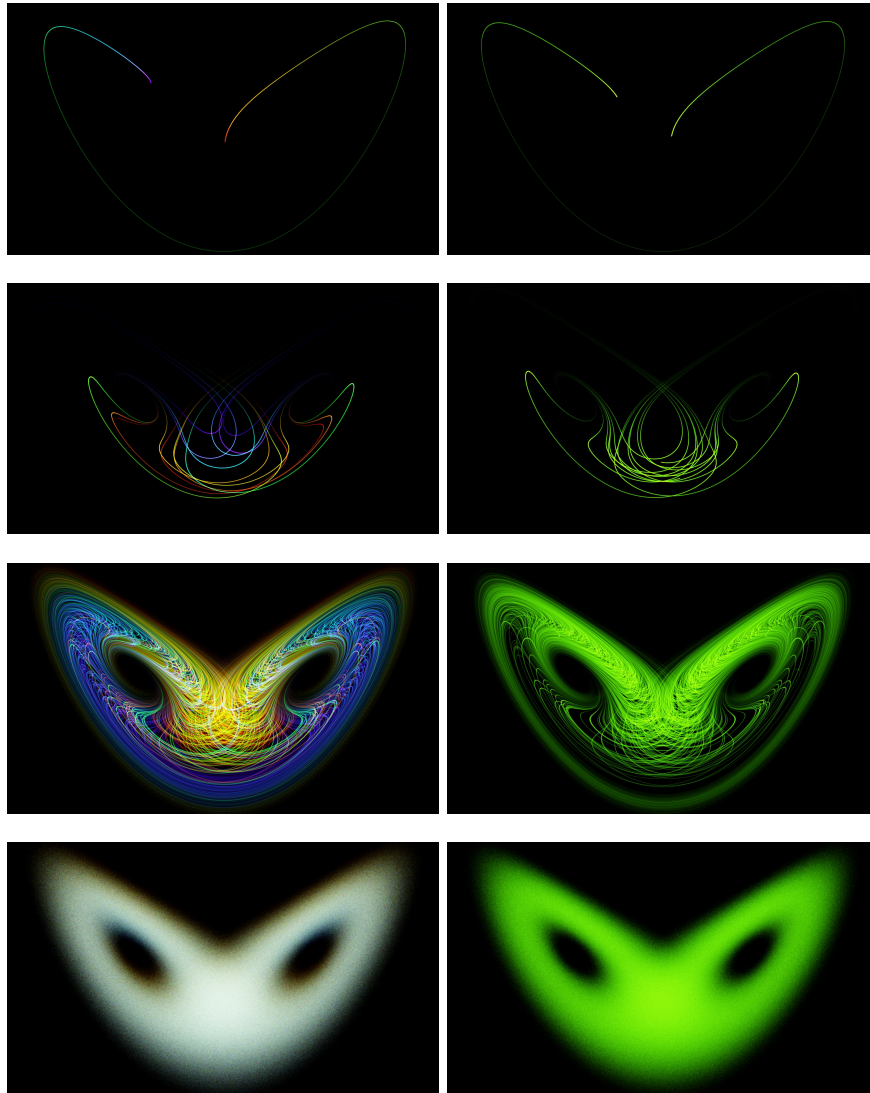


Figure 1: Sensitive dependence of trajectories on: initial value (left) and parameters of governing equations (right). Different colors indicate different parameter values.

$w$  characterizes the kind of perturbation in the right column of figure 1.

Hence  $v^*$  and  $w$  describe the effect of changing  $s$  and  $u_0$ , respectively. Also, equation 4 differs from equation 3 by setting the right hand side to zero. If two different tangent solutions, say  $v^*$  and an arbitrary  $v$ , both satisfies equation 3, their difference is a homogeneous tangent solution  $w$ .

This matches our previous description: changing  $s$  has two effects, one is the same as changing  $u_0$ , the other is shifting the attractor. Since we are interested in the latter, we want to find a  $w$  such that  $v = v^* - w$  characterizes the motion of the attractor. In fact, subtracting such  $w$  from  $v^*$  is the main idea behind NILSS. The criterion of a correct  $v$  is that the magnitude of  $v^\perp$  is small, the reason for which is mentioned in Appendix A.

Here  $v^\perp$  is defined through the orthogonal projection onto  $V^\perp(u)$ , the subspaces perpendicular to  $f(u)$ . This projection gives  $v^\perp$ ,  $w^\perp$ ,  $\Delta u^\perp$ , and  $v^{*\perp}$ , corresponding to  $v$ ,  $w$ ,  $\Delta u$ , and  $v^*$ . For example,  $v^\perp$  is:

$$v^\perp = v - \frac{f^T v}{f^T f} f$$

It is known by the shadowing lemma [28] that such a desired tangent solution  $v^\infty$  exists, but it is challenging to find. The main goal of NILSS is to find a  $w$  such that  $v = v^* - w \approx v^\infty$ . This could be easily done if we could know all Lyapunov Characteristic Vectors (LCV), which is the topic of the next subsection.

### 3.2. Decomposition of the perpendicular subspace $V^\perp$

NI-LSS and conventional LSS both assumes uniform hyperbolicity. But for the simplicity of discussion, we make a stronger assumption in this paper, that is, the dynamical system has a full set of Lyapunov Exponents (LE) and corresponding Lyapunov Characteristic Vectors (LCV). More specifically, there is  $\{\lambda_j\}, j = 1, 2, \dots, m$ , such that for all  $u$  on the attractor and homogeneous tangent solution  $w$ , there is a unique representation of  $w$  as:

$$w = \sum_{j=1}^m a_j(u) \zeta_j(u) \tag{5}$$

Here each  $\zeta_j(u)$  is a homogeneous tangent solution, and its magnitude behaves like exponential functions of time. That is, there exists  $C_1$  and  $C_2$ , such that for any primal  $u(\tau)$  on the attractor, for any  $j$  and  $t$ ,

$$C_1 e^{\lambda_j t} \|\zeta_j(u(0))\| \leq \|\zeta_j(u(t))\| \leq C_2 e^{\lambda_j t} \|\zeta_j(u(0))\| \tag{6}$$

This relation will also be denoted by:

$$\|\zeta_j(u(t))\| \approx e^{\lambda_j t} \|\zeta_j(u(0))\| \tag{7}$$

$\{\lambda_j\}$  and  $\{\zeta_j\}$  are LEs and LCVs, respectively. LCVs with positive  $\lambda_j$  are called unstable modes, while those with negative  $\lambda_j$  is called stable modes. Unstable modes are the reason for ‘butterfly effect’, since a perturbation in the unstable subspace grows exponentially in time.

We further assumes that there is only one zero LE, and its LCV is parallel to  $f(u)$ . We also require that all LCVs are uniformly bounded away from each

other, that is, the angles between any two LCVs are bigger than some  $\alpha_0$  for all  $u$  on the attractor.

Notice that stable and unstable modes are not necessarily in  $V^\perp$ . However, we can project them onto  $V^\perp$ , to obtain a similar decomposition on  $V^\perp(u)$ . For any  $w^\perp \in V^\perp(u)$ ,

$$w^\perp = \sum_{j=1}^m a_j(u) \zeta_j^\perp(u) \quad (8)$$

where  $\zeta_j^\perp(u)$  are orthogonal projection of  $\zeta_j(u)$  onto  $V^\perp(u)$ . We also call  $\zeta_j^\perp$  stable or unstable modes based on their corresponding  $\lambda_j$ .

Since angles between  $\{\zeta_j\}$  and  $f(u)$  are greater than  $\alpha_0$ , the angles between  $\{\zeta_j\}$  and  $V^\perp$  are always smaller than  $\pi/2 - \alpha_0$ . This means the amplitude of  $\{\zeta_j^\perp\}$  still behaves like exponentials:

$$\|\zeta_j^\perp(u(t))\| \approx e^{\lambda_j t} \|\zeta_j^\perp(u(0))\| \quad (9)$$

Notice there are  $(m-1)$  such  $\zeta_j^\perp$  since  $V^\perp(u)$  is a  $(m-1)$  dimensional space. Their corresponding  $\lambda_j$  are all non-zero.

The analytical solution has non-zero initial condition  $v^\infty(0) \neq 0$ , however, conventional tangent solution uses zero initial condition  $v^*(0) = 0$ . The difference between the two initial conditions very likely contains some unstable components. This causes the exponential growth in the magnitude of  $v^*$  and  $v^{*\perp}$ , and the computation failure in the transient method.

Assume that we know each unstable  $\zeta_j^\perp$ , we can subtract from  $v^{*\perp}$  its projection onto each of them. Denote this result by  $v^{L\perp}$ , then  $v^{L\perp} - v^{\infty\perp}$  do not have significant unstable modes. In other words, their difference is mainly stable modes, which decays very fast.  $v^{L\perp}$  obtained in this way satisfies the criterion that  $v^{L\perp}$  is small, and can be used to compute sensitivity.

To achieve the same effect, we only need to know the span of unstable modes, instead of knowing each of them separately. Moreover, subtracting  $\zeta_j^\perp$  from  $v^{*\perp}$  is the same as find the closest point in the affine space  $v^{*\perp} + \text{span}\{\zeta_j^\perp\}$  to the origin. This leads to NILSS method.

### 3.3. Computing bounded $v^\perp$ by NI-LSS

This subsection presents the main part of NILSS, that is, how to find a  $v^\perp$  whose magnitude is as small as possible.

To do this, we minimize the  $L^2$  norm of  $v^{N\perp} = v^{*\perp} + W^\perp a$ :

$$\min_a \frac{1}{2} \int_0^T (v^{*\perp} + W^\perp a)^T (v^{*\perp} + W^\perp a) \quad (10)$$

Here  $W^\perp(t) = \{w_j^\perp(t), j = 1, \dots, p\}$ . The initial condition  $w_j(t=0)$  are randomized bounded vector in  $\mathbb{R}^m$ . The arguments for the optimization problem,  $a$ , is a column vector in  $\mathbb{R}^p$ .

Here  $p$  is an integer larger than the number of positive LEs. In the paper about computing LEs [29], we can see that  $\text{span}\{w_j^\perp\}$  approximately contains

the span of unstable modes. Due to the arguments in last subsection, we know that there exists an  $a$  which could give a desired  $v^\perp$ . Furthermore, due to the minimization, the magnitude of  $v^\perp$  is even smaller than  $v^L$ . Hence the result  $v$  can be used to compute sensitivity. The formalized argument of why  $v^*$  approximates  $v^*$  is beyond the scope of this paper, and it will appear in a different paper.

In the minimization of  $\|v^{N\perp}\|$ , the unstable modes in the error will be suppressed since their magnitudes grow exponentially. On the other hand, the minimization might introduce additional components in stable modes. However, stable modes will decay exponentially hence their impact on the magnitude of  $v$  is negligible. The intuition of the effect of minimization is illustrated in Figure 2.

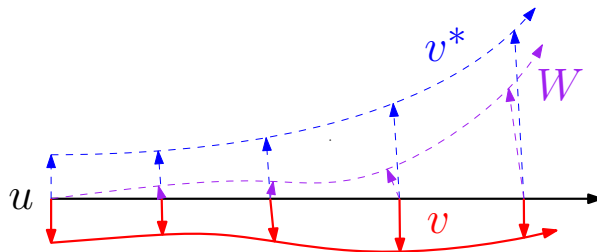


Figure 2:  $v^\perp = v^{*\perp} + W^\perp a$ , want to find a  $v^\perp$  whose magnitude is small.

There are only  $p$  arguments in the minimization problem posed in equation 10, hence the optimization problem in NILSS is very cheap to solve. On the other hand, the main cost in NILSS is in preparing the optimization problem, that is, to compute  $v^{*\perp}$  and  $w_1^\perp(t), \dots, w_p^\perp(t)$ . For problems with a low dimensional attractor, there are fewer unstable modes, hence fewer  $\{w_j\}$  to compute. As a result, NILSS has lower cost.

A beneficial side-effect is that the total amount of data we need to store is less than that of the conventional LSS method. Furthermore, all the tangent solutions used in NILSS need not be put into computer memory at the same time. The formulation of NILSS allows us to put those tangent solutions on hard drive, and read in two tangent solutions sequentially to compute their inner product. This implementation may reduce the computation speed, but saves much computer memory. Also, the optimization problem in equation 10 is very small and requires little memory. To summarize, NILSS could potentially require much less computer memory than conventional LSS.

#### 3.4. Compute $d\langle J \rangle_\infty / ds$ from the tangent solution

Since  $v - v^\perp$  is parallel to  $f$ , we can define

$$\xi f = v - v^\perp \quad (11)$$

To find a pair  $(v^\perp, \xi)$ , first solve equation 3 to get  $v$ , project  $v$  onto subspace  $V^\perp$  to find  $v^\perp$ , then use equation 11 to find  $\xi$ .



Once we obtain a  $v^N$  such that the magnitude of  $v^{N\perp}$  is small, we can compute corresponding  $\xi^N$ . Then we have the following approximation for  $d\langle J \rangle_\infty/ds$ :

$$\frac{d\langle J \rangle_\infty}{ds} \approx \frac{1}{T} \left[ \int_0^T (\partial_u f v^N + \partial_s J) dt + \xi|_0^T \langle J \rangle_T - (\xi J)|_0^T \right] \quad (12)$$

Here  $\langle J \rangle_T$  is as defined in equation 2. Explanation of the above formula is in Appendix A.

#### 4. Tangent NILSS Algorithm

In this section, first we talk about how to avoid  $v^{\perp}$  and  $W^{\perp}$  from becoming too large, by rescaling them after every short segment of time  $\Delta T$ . Then we discuss the criterion for determining  $p$ ,  $T$ , and  $\Delta T$ . Finally, we provide a detailed walk-through of the tangent NILSS algorithm.

A variation of tangent NILSS is the finite difference NILSS. This formulation is obtained by approximating the tangent solutions by finite difference solutions. An explanation of finite difference NILSS could be found in Appendix B.

##### 4.1. Solving NI-LSS on multiple time segments

Since both  $v^{\perp}$  and  $W^{\perp}$  grow exponentially, the round off error will soon become non-negligible. It will also make the covariance matrix  $(W^{\perp})^T W^{\perp}$  singular, since all  $w_j^{\perp}$  will eventually be dominated by the fastest growing unstable direction. This subsection shows how to prevent this by partitioning a long trajectory into several shorter segments.

Partition the time domain into  $n$  time segments  $[t_0, t_1], [t_1, t_2], \dots, [t_{n-1}, t_n]$ , with  $t_0 = 0, t_n = T$ . Define time segment  $i$  as  $[t_i, t_{i+1}], i = 0, \dots, n - 1$ . Then  $v^{\perp}$  and  $W^{\perp}$  become  $\{v_i^{\perp}\}$  and  $\{W_i^{\perp}\}$  for time segment  $i$ . Above notations is also depicted in Figure 3.

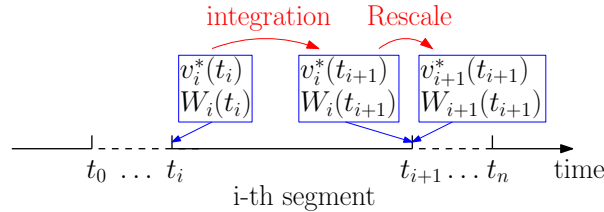


Figure 3: Notations used for tangent NI-LSS,  $t_0 = 0, t_n = T$

We want to rescale  $v^{\perp}$  and  $W^{\perp}$  at the end of each segment so that they do not grow too large. We also want to keep the affine vector space  $v^{\perp} + \text{span}(W^{\perp})$  the same across these segments.:

$$v_i^{\perp}(t_i) + \text{span}(W_i^{\perp}(t_i)) = v_{i-1}^{\perp}(t_i) + \text{span}(W_{i-1}^{\perp}(t_i)) \quad (13)$$

Where  $\text{span}(W^\perp)$  is the vector space spanned by the column vectors of  $W^\perp$ .

To achieve this, first orthonormalize  $W^\perp$  with a QR decomposition:

$$W_i^\perp(t_{i+1}) = Q_i R_i \quad (14)$$

set the initial conditions of the next tangent segment to

$$W_{i+1}^\perp(t_{i+1}) = Q_i \quad (15)$$

In QR factorization, the column vectors in  $Q_i$  and  $W_i^\perp$  could represent each other. Hence  $\text{span}(W_i^\perp(t_i)) = \text{span}(W_{i-1}^\perp(t_i))$

Then use Gram-Schmit for  $v^{*\perp}$ . That is, rescale  $v^{*\perp}$  by subtracting its orthogonal projection on  $W^\perp$  to obtain the initial condition of the next time segment:

$$v_{i+1}^{*\perp}(t_{i+1}) = v_i^{*\perp}(t_{i+1}) - W_{i+1}^\perp(t_{i+1})b_i$$

here  $b_i = W_{i+1}^\perp(t_{i+1})^T v_i^{*\perp}(t_{i+1})$ . Notice that  $v_{i+1}^{*\perp}(t_{i+1})$  is still in the affine space  $v_i^{*\perp}(t_i) + \text{span}(W_i^\perp(t_i))$ .

Now equation 13 is satisfied, for any  $a_{i-1}$ , there exists  $a_i$  such that:

$$v_i^{*\perp}(t_i) + W_i^\perp(t_i)a_i = v_{i-1}^{*\perp}(t_i) + W_{i-1}^\perp(t_i)a_{i-1}$$

Hence we can enforce the continuity requirement on  $\{v_i^{N\perp}\}$ :

$$v_i^{N\perp}(t_i) = v_{i-1}^{N\perp}(t_i) \quad (16)$$

Hence the solution  $v^N$  on multiple time segment is same as that of one longer segment. However, rescaling  $v^{*\perp}$  and  $W^\perp$  at the end of each time segment prevents them from growing too large.

It is not a new idea of using QR factorization to rescale homogeneous solutions while keeping a continuous subspace. In the paper of computing LE [29], the same technique was used.

#### 4.2. Determining parameters for NILSS

There are two parameters in NILSS for users to decide: number of homogeneous solutions and length each of time segments. This subsections briefly talks about how to determine these parameters.

LEs are a by product of NILSS, since our procedure of rescaling  $\{w_j^\perp\}$  at the end of each time segment is exactly the same as that used in computing LEs [29]. To obtain the j-th largest LE, we just need to take average of the j-th diagonal element in  $R_i$  over all  $i = 0, 1, \dots, n-1$ . In practice, we can gradually increase the number of homogeneous solutions until all positive LEs show up. Then we select  $p$  bigger than the number of positive LEs.

On the other hand, we want to partition the whole trajectory so that the LCV with the largest LE do not dominate the  $p$ -th LCV. Otherwise the covariance matrix grows singular, since all  $\{w_j^\perp\}$  will be almost parallel to the LCV with largest LE. Assume the largest LE is  $\lambda_{max}$ , and  $p$ -th LE is  $\lambda_p$ . We want to rescale  $W^\perp$  and  $v^{*\perp}$  after time span  $\Delta T \leq (\lambda_{max} - \lambda_p)^{-1}$ . This relation determines how we select  $\Delta T$ . Note that in general  $\lambda_{min+} \neq \lambda_p$ .

### 4.3. Pre-process

From here on we look at the detailed algorithm of NILSS.

First integrate equation (1) for some time, and then set  $t = 0$ , so that  $u$  is on the attractor at the beginning of our algorithm. Next, integrate equation (1) from  $t = 0$  to  $T$ , to obtain the primal solution  $u(t)$ .

### 4.4. Compute the homogeneous solution $\{W_i\}$

We solve  $p$  tangent equations on each of the  $n$  time segments  $[t_0, t_1], \dots, [t_{n-1}, t_n]$ , with  $t_0 = 0, t_n = T$ . Time segment  $i$  is the time span  $[t_i, t_{i+1}]$ . This notation is the same as that in Figure 3.

We start at the first time segment with random initial conditions  $W_0(0) = [w_{0,1}(0), \dots, w_{0,p}(0)]$ , where  $w_{0,j}(0) \in V^\perp(u(0))$ . Then proceed with the following algorithm starting at  $i = 0$ .

1. Starting from the initial conditions

$$W_i(t_i) = [w_{i,1}(t_i), \dots, w_{i,p}(t_i)],$$

integrate the homogeneous equations to obtain

$$W_i(t_{i+1}) = [w_{i,1}(t_{i+1}), \dots, w_{i,p}(t_{i+1})].$$

2. Computes the orthogonal projection onto  $V^\perp$ :

$$W_i^\perp = [w_{i,1}^\perp, \dots, w_{i,p}^\perp],$$

Meanwhile, compute and store

$$C_i = \int_{t_i}^{t_{i+1}} (W_i^\perp)^T W_i^\perp dt.$$

3. Orthonormalize  $W_i^\perp(t_{i+1})$  with a QR decomposition:

$$W_i^\perp(t_{i+1}) = Q_i R_i.$$

$R_i$  and  $Q_i$  can also be computed through Cholesky decomposition of  $W_i^\perp(t_{i+1})^T W_i^\perp(t_{i+1})$ . Store  $R_i$  and set the initial conditions of the next tangent segment to

$$W_{i+1}(t_{i+1}) = Q_i.$$

4. Let  $i = i + 1$ . Go to Step 1 unless  $i$  is greater than  $n - 1$ , in which case the algorithm terminates.

4.5. Compute the inhomogeneous solution  $\{v_i^*\}$

We start at the first time segment with a zero initial condition  $v_0^*(0) = 0$ . Proceed with the following algorithm starting at  $i = 0$ .

1. Starting from the initial condition  $v_i^*(t_i)$ , integrate the inhomogeneous equations to obtain  $v_i^*(t_{i+1})$ . Then compute the orthogonal projection,  $v_i^{*\perp}$ . Meanwhile, compute and store

$$d_i = \int_{t_i}^{t_{i+1}} W_i^{\perp T} v_i^{*\perp} dt,$$

2. Orthogonalize  $v_i^{*\perp}(t_{i+1})$  with respect to  $W_{i+1}^{\perp}(t_{i+1})$  via Gram-Schmidt procedure to obtain the initial condition of the next time segment:

$$v_{i+1}^*(t_{i+1}) = v_i^{*\perp}(t_{i+1}) - W_{i+1}^{\perp}(t_{i+1})b_i$$

where

$$b_i = W_{i+1}^{\perp}(t_{i+1})^T v_i^{*\perp}(t_{i+1})$$

should be stored.

3. Let  $i = i + 1$ . Go to Step 1 unless  $i$  is greater than  $n - 1$ , for which case the algorithm terminates.

Here we present solving inhomogeneous solution  $v_i^*$  as a separate step after the homogeneous solution  $W_i$ . They can also be integrated simultaneously.

4.6. Compute the NILSS tangent,  $v^N$

The arguments of the minimization problem in tangent NILSS are  $a_i \in \mathbb{R}^p, i = 0, \dots, n - 1$ . The minimum norm statement is now minimizing

$$\sum_{i=0}^{n-1} \int_{t_i}^{t_{i+1}} [(v_i^{*\perp})^T v_i^{*\perp} + 2(v_i^{*\perp})^T W_i^{\perp} a_i + a_i^T (W_i^{\perp})^T W_i^{\perp} a_i] dt$$

Other than a constant contribution from  $(v_i^{*\perp})^T v_i^{*\perp}$ , we should choose  $a_i$ 's as

$$\min_{\{a_i\}} \sum_{i=0}^{n-1} 2d_i^T a_i + a_i^T C_i a_i. \quad (17)$$

The continuity of  $v^{N\perp}$  across  $t_i$  can be written as

$$v_{i-1}^{*\perp}(t_i) + W_{i-1}^{\perp}(t_i)a_{i-1} = v_i^{*\perp}(t_i) + W_i^{\perp}(t_i)a_i$$

Consider the relationship of  $v_{i-1}^{*\perp}$  to  $v_i^{*\perp}$  and  $W_{i-1}^{\perp}$  to  $W_i^{\perp}$  at  $t_i$ , the above continuity requirement transforms into:

$$v_i^{*\perp}(t_i) + W_i^{\perp}(t_i)b_{i-1} + W_i^{\perp}(t_i)R_{i-1}a_{i-1} = v_i^{*\perp}(t_i) + W_i^{\perp}(t_i)a_i$$

Which is equivalent to:

$$a_i = R_{i-1}a_{i-1} + b_{i-1} \quad (18)$$

Combining the minimization problem in equation (17) and the continuity constraints in equation (18), we obtain the constraint least squares problem:

$$\begin{aligned} \min_{\{a_i\}} \sum_{i=0}^{n-1} 2d_i^T a_i + a_i^T C_i a_i \\ \text{s.t. } a_i = R_{i-1}a_{i-1} + b_{i-1} \quad i = 1, \dots, n-1, \end{aligned} \quad (19)$$

Once  $\{a_i\}$  is obtained by solving equation (19), we can compute  $v_i^N$  within each time interval  $t \in [t_i, t_{i+1}]$  by:

$$v_i^N(t) = v_i^*(t) + W_i(t)a_i \quad (20)$$

Notice that here  $v_i^N$  is not continuous across the  $t_i$ , but  $v_i^{N\perp}$  is. The number of arguments in this minimization problem is  $p \times n$ , which is smaller than conventional LSS.

#### 4.7. Compute $\xi_i$

At the beginning of each segment,  $v^*$  and  $W$  are in  $V^\perp$ , hence so is  $v^N$ . As a result,

$$\begin{aligned} \xi_i(t_i) &= 0 \\ \xi_i(t_{i+1}) &= \frac{(v_i^N(t_{i+1}))^T f(u(t_{i+1}))}{f(u(t_{i+1}))^T f(u(t_{i+1}))} f(u(t_{i+1})) \end{aligned} \quad (21)$$

#### 4.8. Compute $d\langle J \rangle / ds$

Once  $v^N(t)$  is obtained,  $d\langle J \rangle_\infty / ds$  is computed by

$$\frac{1}{T} \sum_{i=0}^{n-1} \int_{t_i}^{t_{i+1}} (\partial_u f v_i^N + \partial_s J) dt + \xi_i(t_{i+1})(\langle J \rangle_T - J(T)) \quad (22)$$

To derive equation 22 from equation 12, notice that a continuous  $\xi$  could be recovered by ‘accumulating’ all previous  $\xi_i$ , that is:

$$\xi(t) = \xi_i(t) + \sum_{i'=0}^{i-1} \xi_{i'}(t_{i'+1}), \quad t \in [t_i, t_{i+1}]$$

Alternatively, the sensitivity can be computed without explicitly forming  $v^N(t)$ . The sensitivity contribution of  $v^N$  within each time interval can be computed from  $v_i^*$  and  $w_{i,j}$  when they are solved, and a linear combination of them, with  $a_i$  being the coefficients.

## 5. Numerical Results on Lorenz attractor

We apply the tangent NILSS to the Lorenz 63 system. It has three states, that is,  $m = 3$ , and the governing equation is:

$$\frac{dx}{dt} = \sigma(y - x), \quad \frac{dy}{dt} = x(\rho - z) - y, \quad \frac{dz}{dt} = xy - \beta z \quad (23)$$

In our current numerical example, we set  $\sigma = 10, \beta = 8/3$ . The parameter of the system is  $\rho$ , which vary in range  $[2, 45]$ . The Lorenz 63 system has different behaviors[30] when  $\rho$  changes :

- $2 \leq \rho < 24.7$ , two stable point attractors.
- $24.7 \leq \rho < 31$ , one quasi-hyperbolic strange attractor.
- $31 \leq \rho \leq 45$ , one non-hyperbolic attractor.

For our study, we select the quantity of interest to be:

$$\langle J \rangle = \lim_{T \rightarrow \infty} \frac{1}{T} \int_0^T z dt$$

When solving the primal solution  $u = (x, y, z)^T$ , we use Euler forward integration with time step size 0.005. We perform NI-LSS with  $T = 100$ , divided into  $n = 20$  segments. Number of unstable directions is  $m_{us} = 1$ , and we set  $p = 1$ .

The resulting  $\langle J \rangle$  and  $\frac{d\langle J \rangle}{d\rho}$  is shown in Figure 4 and Figure 5.

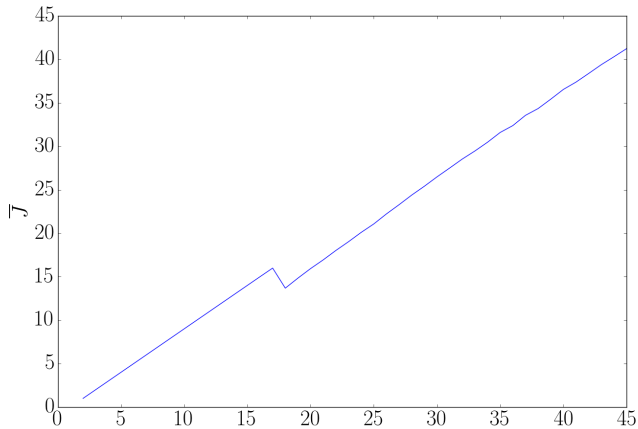


Figure 4:  $\langle J \rangle$  computed for each  $\rho$ , averaged over 100 time units.

It has been shown that the true value of  $\frac{d\langle J \rangle}{d\rho}$  is about 1 for all  $\rho$ , which could also be observed from figure 4. The sensitivities computed with NI-LSS match this result, as can be seen in Figure 5.

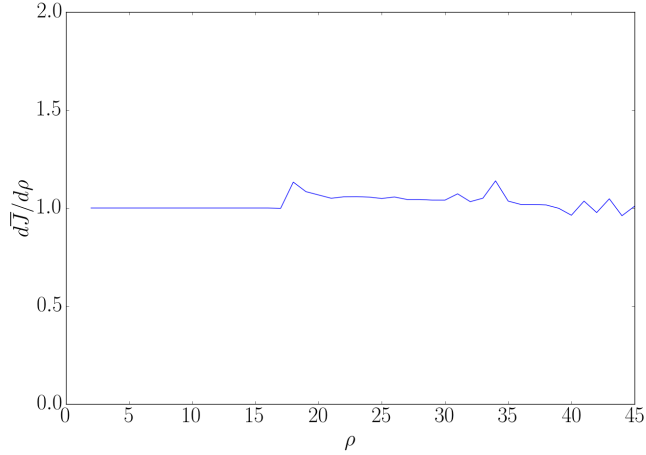


Figure 5:  $\frac{d(J)}{d\rho}$  computed for each  $\rho$  using tangent NILSS. The time length of trajectories is  $T = 100$ , and the whole time span is partitioned into 20 segments of length 5.

## 6. Numerical Results on CFD Simulation of flow over a backward facing step

We verify NILSS on the test case in the tutorial of OpenFOAM [31], which is modeled from the experiment by Pitz and Daily [32]. This problem is 2 dimensional flow with a backward step at the inlet and a contracting nozzle at the outlet, as shown in figure 7. The flow is chaotic but not turbulent, since it's two dimensional.

We set no-slip wall condition for all boundaries except for the inlet and outlet. We set outlet with fixed pressure  $p = 0Pa$ . The inlet boundary condition is fixed velocity in x-direction, the magnitude of which is the parameter to be perturbed. For the base case, we set inlet velocity  $U = (10, 0, 0)m/s$ .

For the numerical simulation, we solve incompressible Navier-Stokes equation by pisoFOAM. We use 2nd order finite volume scheme; the time-integration method is PISO (Pressure Implicit with Splitting of Operator), time step size is  $1 \times 10^{-5}$  second. Originally the inlet used a turbulence inlet boundary condition, which is generated randomly for each simulation. To make sure that the objective solely depend on the parameter, we use a uniform fixed value boundary condition. We use the mesh as provided in the tutorial, which is shown in figure 6. A typical snapshot of the flow field is shown in figure 7.

To get the long-time averaged objective, we perform simulation over  $2 \times 10^5$  time steps. To get the uncertainty of the objective, we divide the simulation into 5 equally long parts, and take average over the objective of each part. We compute the standard error of these 5 averages. Since here we assume that the standard error is proportional to  $T^{-0.5}$ , we divide the above result by  $\sqrt{5}$  as

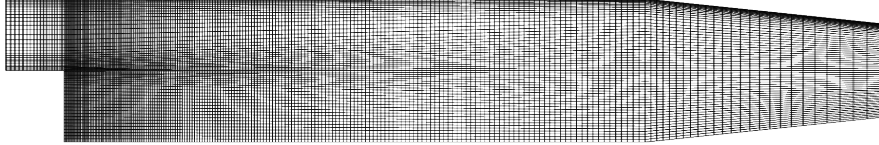


Figure 6: Mesh of test case

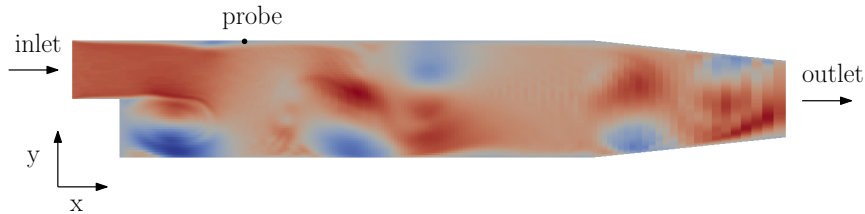


Figure 7:  $U_x$  at time 0.091

the standard error of the averaged objective of the whole trajectory. Objectives for difference parameters in range [9,11] are shown in figure 8, where the bar indicates the 95% confidence interval.

For the sensitivity analysis, we set the parameter to be the x-direction velocity at the inlet,  $U_{x0}$ . We use four different objectives: the long time average of  $U_x/U_{x0}$ ,  $(U_x/U_{x0})^2$ ,  $(U_x/U_{x0})^4$ , and  $(U_x/U_{x0})^8$ . Here  $U_x$  is the x-direction velocity at a probe, the location of which is shown in figure 7. For NILSS, we use finite difference to approximate tangent solutions, as explained in Appendix B. Set  $p = 16$ , which is larger than the number of positive LEs, 8. Each segment has 250 time steps. To compute the sensitivity, we run NILSS for 200 segments. The total time steps computed in NILSS is  $200 \times 250 \times 18 = 9 \times 10^5$ . The sensitivity solution for parameter  $U_{x0} = 10$  is shown in figure 8.

$dJ/ds$  converges to the true sensitivity as we increase  $T$ . The left column in figure 8 is the log-log plot of  $dJ/ds(T)$ . Assume that the confidence interval of NILSS is also proportional to  $T^{-0.5}$ . For some  $(dJ/ds)_0$ , define  $C$  as the smallest number satisfies:

$$(dJ/ds)_0 - dJ/ds(T') \leq CT'^{-0.5}, \text{ for all } T'$$

To find the confidence interval of  $(dJ/ds)$ , we vary  $(dJ/ds)_0$  such the corresponding  $C$  is smallest. Then  $CT^{-0.5}$  is regarded as the confidence interval



for the sensitivity computed by NILSS. The lines in the left column indicate  $CT^{-0.5}$ , and the wedges in the right column indicate the confidence interval of sensitivity computed by NILSS. As we can see, the sensitivity computed by NILSS correctly reflects the trend in long-time averaged objectives.

The cost of NILSS is lower than that of the conventional finite difference method. For conventional finite difference method, we do a linear regression of the objectives over 5 parameters; the total number of time steps computed is  $5 \times 2 \times 10^5 = 1 \times 10^6$ . Now the cost of NILSS and conventional finite difference are roughly the same. However, in figure 8, the distance between parameters is 1. Considering that the base parameter is only 10, this variation is too large for conventional finite difference. If we want the parameters be closer to each other, smaller confidence intervals for objectives are needed. Assume the size of confidence interval is proportional to  $T^{-0.5}$ . If we want to use a smaller parameter difference of 0.1, then we need to decrease the confidence interval size by the same factor. This means that the primal solution should be 100 times longer, which would greatly raise the cost of the conventional finite difference.

When there are multiple parameters, the cost of NILSS is even lower than conventional finite difference method. In NILSS, equation 3 has right hand side  $\partial_s f$ , which says  $v^*$  would change if we have a new parameter. However,  $w_j$  does not depend on  $s$ , so they could be reused for the new parameter. In our finite difference version, this means we can reuse the base primal solution and the solution with perturbed initial conditions. So the marginal cost of another parameter is only 1/18 of the cost of the first parameter. On the other hand, for conventional finite difference, the marginal cost is 4/5 of that of the first parameter, since only the base primal solution could be reused, while all other perturbed solutions should be recomputed.

## 7. Conclusions

The tangent Non-Intrusive Least Square Shadowing (NILSS) has several advantages:

1. It potentially requires only minor modifications to existing tangent solvers.
2. For problems with a low dimensional attractor, which is the case for many engineering applications, NILSS has lower cost than the conventional finite difference method and the conventional LSS method.
3. NILSS requires less computer memory than the conventional LSS.

NILSS has been demonstrated on the Lorenz 63 system and a CFD simulation for a flow over a backward facing step. In both cases, NILSS gives the correct sensitivity. For the latter case, NILSS has roughly same computational cost as computing an long-time averaged objective, which is lower than both the conventional finite difference and the conventional LSS method.

The python code that implemented the algorithm introduced in this paper are available at [github.com/qiqi/fds](https://github.com/qiqi/fds).

## References

## References

- [1] A. N. Kolmogorov, The Local Structure of Turbulence in Incompressible Viscous Fluid for Very Large Reynolds Numbers, *Proceedings: Mathematical and Physical Sciences* 434 (1890) (1991) 9–13.  
URL <http://www.jstor.org/stable/51980>
- [2] E. Dowell, Flutter of a buckled plate as an example of chaotic motion of a deterministic autonomous system, *Journal of Sound and Vibration* (1982) 333–344.  
URL <http://www.sciencedirect.com/science/article/pii/0022460X82902590>
- [3] P. Walters, *An introduction to ergodic theory*, Vol. 79, Springer Science & Business Media, 2000.
- [4] A. Jameson, Aerodynamic design via control theory, *Journal of scientific computing* 3 (3) (1988) 233–260.
- [5] J. J. Reuther, A. Jameson, J. J. Alonso, M. J. Rimlinger, D. Saunders, Constrained Multipoint Aerodynamic Shape Optimization Using an Adjoint Formulation and Parallel Computers, Part 2, *Journal of Aircraft* 36 (1) (1999) 61–74. doi:10.2514/2.2414.  
URL <http://arc.aiaa.org/doi/abs/10.2514/2.2414>
- [6] T. R. Bewley, Flow control: new challenges for a new Renaissance, *Progress in Aerospace Sciences* 37 (2001) 21–58.  
URL <http://turbulence.ucsd.edu>.
- [7] T. R. Bewley, P. Moin, R. Temam, DNS-based predictive control of turbulence: an optimal benchmark for feedback algorithms, *Journal of Fluid Mechanics* 447 (2001) 179–225. doi:10.1017/S0022112001005821.
- [8] J. Tromp, C. Tape, Q. Liu, Seismic tomography, adjoint methods, time reversal and banana-doughnut kernels, *Geophys. J. Int* doi:10.1111/j.1365-246X.2004.02453.x.
- [9] R. Becker, R. Rannacher, An optimal control approach to a posteriori error estimation in finite element methods, *Acta Numerica* 10. doi:10.1017/S0962492901000010.  
URL [http://www.journals.cambridge.org/abstract/\\_S0962492901000010](http://www.journals.cambridge.org/abstract/_S0962492901000010)
- [10] M. B. Giles, E. Süli, Adjoint methods for PDEs: a posteriori error analysis and postprocessing by duality, *Acta Numerica* 11. doi:10.1017/S096249290200003X.  
URL [http://www.journals.cambridge.org/abstract/\\_S096249290200003X](http://www.journals.cambridge.org/abstract/_S096249290200003X)

- [11] K. J. Fidkowski, D. L. Darmofal, Review of Output-Based Error Estimation and Mesh Adaptation in Computational Fluid Dynamics [doi:10.2514/1.J050073](https://doi.org/10.2514/1.J050073).
- [12] J.-N. Thepaut, P. Courtier, Four-dimensional variational data assimilation using the adjoint of a multilevel primitive-equation model, *Quarterly Journal of the Royal Meteorological Society* 117 (502) (1991) 1225–1254. [doi:10.1002/qj.49711750206](https://doi.org/10.1002/qj.49711750206).  
URL <http://doi.wiley.com/10.1002/qj.49711750206>
- [13] P. Courtier, J. Derber, R. Errico, J. Louis, T. Vukićević, Important literature on the use of adjoint, variational methods and the Kalman filter in meteorology (oct 1993). [doi:10.1034/j.1600-0870.1993.t01-4-00002.x](https://doi.org/10.1034/j.1600-0870.1993.t01-4-00002.x).  
URL <http://tellusa.net/index.php/tellusa/article/view/14898>  
[http://onlinelibrary.wiley.com/doi/10.1034/j.1600-0870.1993.t01-4-00002.x/abstract\\$%5Cdelimiter%26E30F\\$%5Cnhttp://www.blackwell-synergy.com/doi/abs/10.1034/j.1600-0870.1993.t01-4-00002.x](http://onlinelibrary.wiley.com/doi/10.1034/j.1600-0870.1993.t01-4-00002.x/abstract$%5Cdelimiter%26E30F$%5Cnhttp://www.blackwell-synergy.com/doi/abs/10.1034/j.1600-0870.1993.t01-4-00002.x)
- [14] Q. Wang, R. Hu, P. Blonigan, Least Squares Shadowing sensitivity analysis of chaotic limit cycle oscillations, *Journal of Computational Physics* 267 (2014) 210–224.
- [15] D. J. Lea, M. R. Allen, T. W. N. Haine, Sensitivity analysis of the climate of a chaotic system, *Tellus Series a-Dynamic Meteorology and Oceanography* 52 (5) (2000) 523–532. [doi:10.1256/qj.01.180](https://doi.org/10.1256/qj.01.180).
- [16] G. L. Eyink, T. W. N. Haine, D. J. Lea, Ruelle’s linear response formula, ensemble adjoint schemes and Lévy flights, *Nonlinearity* 17 (5) (2004) 1867.
- [17] J. Thuburn, Climate sensitivities via a FokkerPlanck adjoint approach, *Quarterly Journal of the Royal Meteorological Society* 131 (605) (2005) 73–92. [doi:10.1256/qj.04.46](https://doi.org/10.1256/qj.04.46).  
URL <http://doi.wiley.com/10.1256/qj.04.46>
- [18] T. N. Palmer, A nonlinear dynamical perspective on model error: A proposal for non-local stochastic-dynamic parametrization in weather and climate prediction models, *Quarterly Journal of the Royal Meteorological Society* 127 (572) (2001) 279–304. [doi:10.1002/qj.49712757202](https://doi.org/10.1002/qj.49712757202).  
URL <http://doi.wiley.com/10.1002/qj.49712757202>
- [19] L.-S. Young, What are SRB measures, and which dynamical systems have them?, *Journal of Statistical Physics* 108 (5) (2002) 733–754.
- [20] C. E. Leith, Climate Response and Fluctuation Dissipation, *Journal of the Atmospheric Sciences* 32 (10) (1975) 2022–2026. [doi:10.1175/1520-0469\(1975\)032<2022:CRAFD>2.0.CO;2](https://doi.org/10.1175/1520-0469(1975)032<2022:CRAFD>2.0.CO;2).  
URL [http://journals.ametsoc.org/doi/abs/10.1175/1520-0469\(1975\)032<2022:CRAFD>2.0.CO;2](http://journals.ametsoc.org/doi/abs/10.1175/1520-0469(1975)032<2022:CRAFD>2.0.CO;2)

- [21] R. V. Abramov, A. J. Majda, Blended response algorithms for linear fluctuation-dissipation for complex nonlinear dynamical systems, *Nonlinearity* 20 (12) (2007) 2793.
- [22] R. V. Abramov, A. J. Majda, New Approximations and Tests of Linear Fluctuation-Response for Chaotic Nonlinear Forced-Dissipative Dynamical Systems, *Journal of Nonlinear Science* 18 (3) (2008) 303–341. doi:10.1007/s00332-007-9011-9.  
URL <http://link.springer.com/10.1007/s00332-007-9011-9>
- [23] Q. Wang, Convergence of the least squares shadowing method for computing derivative of ergodic averages, *SIAM Journal on Numerical Analysis* 52 (1) (2014) 156–170.
- [24] P. Blonigan, S. Gomez, Q. Wang, Least Squares Shadowing for sensitivity analysis of turbulent fluid flows, in: 52nd Aerospace Sciences Meeting, 2014, pp. 1–24. arXiv:1401.4163.  
URL <http://arxiv.org/abs/1401.4163>
- [25] P. J. Blonigan, Least Squares Shadowing for Sensitivity Analysis of Large Chaotic Systems and Fluid Flows, Ph.d thesis, MIT (2016).
- [26] P. J. Blonigan, Q. Wang, E. J. Nielsen, B. Diskin, Least Squares Shadowing Sensitivity Analysis of Chaotic Flow around a Two-Dimensional Airfoil, in: 54th AIAA Aerospace Sciences Meeting, no. January, 2016, pp. 1–28. doi:10.2514/6.2016-0296.  
URL <http://arc.aiaa.org/doi/10.2514/6.2016-0296>
- [27] E. N. Lorenz, Deterministic Nonperiodic Flow, *Journal of the Atmospheric Sciences* 20 (2) (1963) 130–141. doi:10.1175/1520-0469(1963)020<0130:DNF>2.0.CO;2.  
URL [http://journals.ametsoc.org/doi/abs/10.1175/1520-0469\(1963\)281963\(1963\)29020\(1963\)3C0130\(1963\)3ADNF\(1963\)3E2.0.CO\(1963\)3B2](http://journals.ametsoc.org/doi/abs/10.1175/1520-0469(1963)281963(1963)29020(1963)3C0130(1963)3ADNF(1963)3E2.0.CO(1963)3B2)
- [28] S. Y. Pilyugin, Shadowing in Dynamical Systems, *Lecture Notes in Mathematics*. doi:10.1007/BFb0093184.
- [29] G. Benettin, L. Galgani, A. Giorgilli, J.-M. Strelcyn, Lyapunov Characteristic Exponents for smooth dynamical systems and for hamiltonian systems; A method for computing all of them. Part 2: Numerical application, *Mechanica* 15 (1) (1980) 21–30. doi:10.1007/BF02128237.  
URL <http://dx.doi.org/10.1007/BF02128237>
- [30] C. Sparrow, *The Lorenz equations: bifurcations, chaos, and strange attractors*, Vol. 41, Springer Science & Business Media, 2012.
- [31] G. Tabor, H. G. Weller, H. Jasak, C. Fureby, A tensorial approach to computational continuum mechanics using object-oriented techniques, *Computers in Physics* 12 (6) (1998) 620–631. doi:10.1063/1.168744.

- [32] R. W. Pitz, J. Daily, Combustion in a turbulent mixing layer formed at a rearward facing step, AIAA Journal 21 (11) (1983) 1565–1570.

### Appendix A. Derive $d\langle J \rangle/ds$

With a perturbation in  $s$ , the governing equation for  $u$  is:

$$\frac{d(u + \Delta u)}{dt} = f(u + \Delta u, s + \Delta s)$$

As shown in fig A.9, assume that at time  $t$ , the difference of the new trajectory from the original one is  $\Delta u^\perp(t)$ . After  $\Delta t$ , neglecting higher order small quantities, this difference becomes  $\Delta u^\perp(t) + (\partial_u f \Delta u^\perp(t) + \partial_s f \Delta s) \Delta t$ . The projection of this new difference onto  $V^0(t + \Delta t)$  is denoted by  $-\eta f \Delta t \Delta s$ ; the projection onto  $V^\perp$  is  $\Delta u^\perp(t + \Delta t)$ .

Recall our definition of  $v$  and  $v^\perp$ , the equation for  $\eta$  is:

$$\frac{dv^\perp}{dt} = \partial_u f v^\perp + \partial_s f + \eta f \tag{A.1}$$

Subtract equation A.1 from 3, we get:

$$\frac{d(v - v^\perp)}{dt} = \partial_u f (v - v^\perp) - \eta f$$

By our definition of  $\xi$ ,

$$\frac{d(\xi f)}{dt} = \partial_u f (\xi f) - \eta f$$

by Leibniz rule for differential,

$$\frac{d(\xi f)}{dt} = \xi \frac{df}{dt} + \frac{d\xi}{dt} f$$

Recall the chain rule for differential,

$$\partial_u f (\xi f) = \xi \partial_u f (f) = \xi (\partial_u f \frac{du}{dt}) = \xi \frac{df}{dt}$$

Finally, we find that  $\eta$  is indeed:

$$\eta = -\frac{d\xi}{dt} \tag{A.2}$$

Above we looked at how to compare the new and base trajectories within the same amount of time  $\Delta t$ . But if we always compare the two trajectories at the same time frame, soon they will part from each other. This would make the higher order small quantities no longer negligible, hence our following analysis not working.

Alternatively, we vary  $\Delta t$  so that the states of the two trajectories remain close. In time  $\Delta t$ , the new trajectory moves a length of  $f \Delta t - \eta f \Delta t \Delta s$ . So the

new speed is  $(1 - \eta\Delta s)f$ . Hence the new trajectory needs time  $\Delta t/(1 - \eta\Delta s) \approx \Delta t(1 + \eta\Delta s)$  to cross the same length  $f\Delta t$ . At this time, the distance between the two trajectories is  $\Delta u^\perp(t + \Delta t)$ . If we can find a bounded  $v^\perp$ ,  $\Delta u^\perp$  will always be in the same order of  $\Delta s$ . In other words, if we compare trajectories at different time frames, the points we are comparing can remain close to each other in the phase space.

The  $J_{new}\Delta t_{new}$  on this small section of new trajectory is:

$$\begin{aligned} & J_{new}\Delta t_{new} \\ &= (J + \partial_u J \Delta u^\perp)(1 + \eta\Delta s)\Delta t \\ &= J\Delta t + \partial_u J \Delta u^\perp \Delta t + J\eta\Delta s \Delta t \end{aligned} \quad (\text{A.3})$$

Integrate above equation over time period  $[0, T]$  and neglect higher order small quantities, the difference in averaged  $J$  is:

$$\begin{aligned} & \frac{1}{T_{new}} \int_0^{T_{new}} J_{new} dt - \frac{1}{T} \int_0^T J dt \\ &= \frac{1}{\int_0^T (1 + \eta\Delta s) dt} \int_0^T (J + \partial_u J \Delta u^\perp + J\eta\Delta s) dt - \frac{1}{T} \int_0^T J dt \\ &= \frac{\Delta s}{T} \int_0^T [\partial_u f v^\perp + \partial_s J + \eta(J - \langle J \rangle)] dt \end{aligned} \quad (\text{A.4})$$

Let  $\Delta s \rightarrow 0$ , we have the formula for  $d\langle J \rangle_\infty/ds$ :

$$\frac{d\langle J \rangle_\infty}{ds} \approx \frac{1}{T} \int_0^T [\partial_u f v^\perp + \partial_s J + \eta(J - \langle J \rangle_T)] dt \quad (\text{A.5})$$

The approximation is due to we are not integrating over an infinitely long trajectory. Apply equation A.2, we can see this is exactly the formula in equation 12.

From this deduction we can see why we want  $v^\perp$  to be small: our analysis requires neglecting higher order small quantities. If  $v^\perp$  grows exponentially, our analysis here is no long valid.

## Appendix B. Finite difference NILSS method

We can use finite difference results to approximate all the tangent solutions used in NILSS method. In fact, we only need to approximate  $v^*$  and  $W$ . Once their approximations are obtained, other parts of the algorithm follow.

To achieve this, first we compute a baseline primal solution  $u_b$ , which satisfies equation 1 with initial condition  $u_0$ . Here  $u_0$  is an arbitrary state on the attractor. Then we change  $s$  to  $s + \Delta s$ , and solve for  $u^*$ , which satisfies the perturbed governing equation with the same initial condition  $u_0$ . Now we have approximation for  $v^*$ :

$$v^* \approx \frac{u^* - u_b}{\Delta s}$$

We solve for  $u^w$  by keeping same  $s$  but use initial conditions  $u_0 + \Delta u_0$ , where  $\Delta u_0$  is random perturbation. The approximation for a homogeneous tangent solution  $w$  is:

$$w \approx u^w - u_b$$

Notice that we can scale  $w$  arbitrary since it is homogeneous solution.

The benefit of this finite difference version of NILSS is that it is truly non-intrusive. In fact, it even no longer requires a tangent solver, all it needs is a simulation software which can solve for the primal solution.

The python package for this finite difference NILSS, `fds`, is available on Github. It also implemented the tangent version of NILSS.

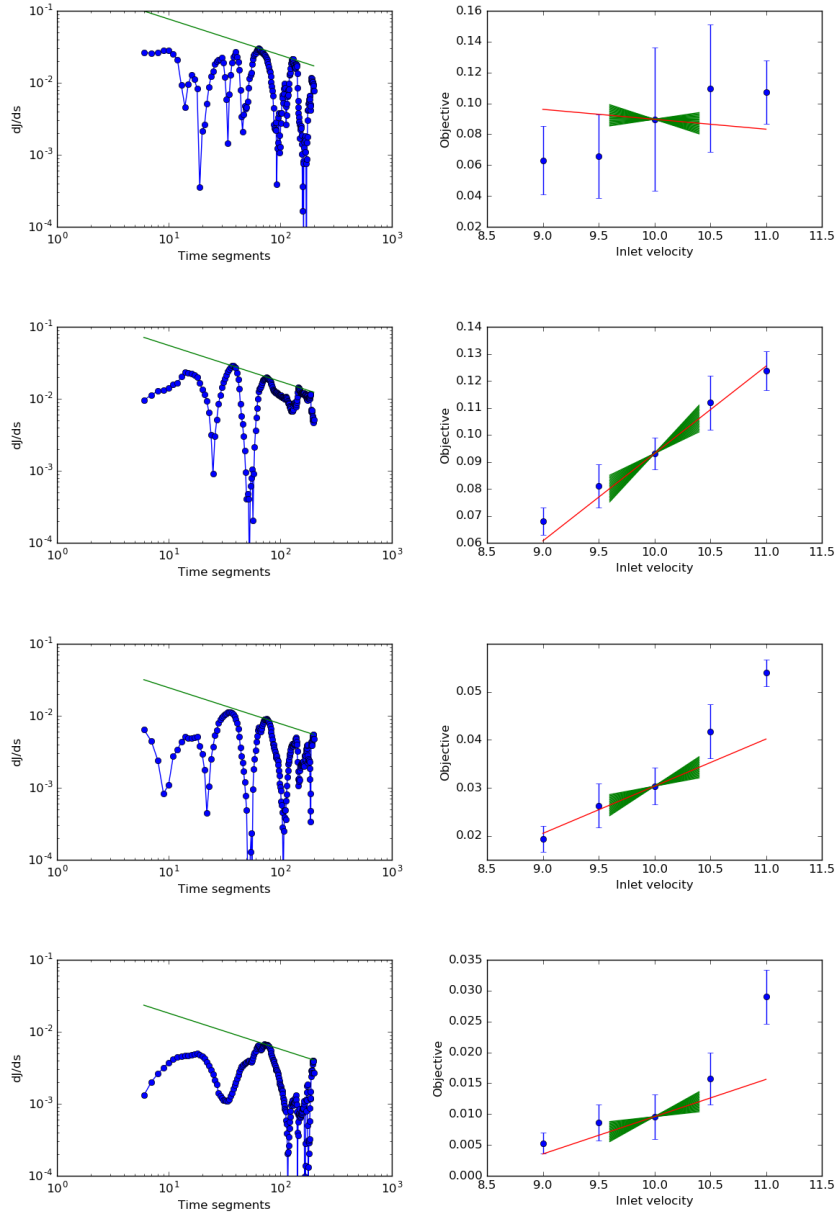


Figure 8: Sensitivity computed by NILSS. From top to bottom the objective function is the long-time average of  $U_x/U_{x0}$ ,  $(U_x/U_{x0})^2$ ,  $(U_x/U_{x0})^4$ , and  $(U_x/U_{x0})^8$ . Left column: sensitivity computed by increasing number of segments, the lines indicates confidence interval for sensitivity. Right column: sensitivity plotted with objectives for adjacent parameters, the bars and wedges indicate confidence intervals of the objectives and sensitivities, respectively.



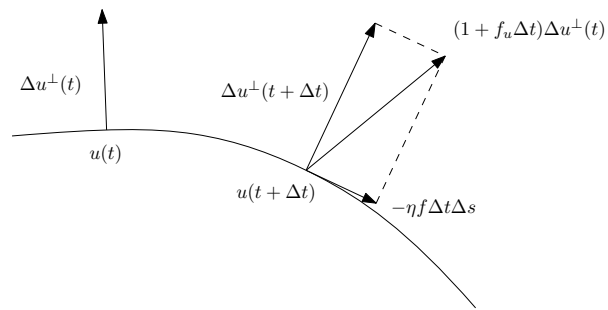


Figure A.9: Perturbation on the trajectory due to perturbation on the parameter